

Supplementary Information for
Structure and thermal boundary resistance of basal plane twin boundaries in Bi₂Te₃

Tables S1, S2, and S3 describe the size of simulation cell utilised for reverse non-equilibrium molecular dynamics (rNEMD) simulations of bulk Bi₂Te₃ and the Te2 twin boundary in Bi₂Te₃.

Table S1: System sizes for reverse non-equilibrium molecular dynamics simulations of the in-plane direction in bulk Bi₂Te₃.

Number of Unit Cells	Length (L_z) (nm)	Number of Atoms
280	≈123	302400
340	≈149	367200
400	≈175	432000
460	≈202	496800

Table S2 System sizes for reverse non-equilibrium molecular dynamics simulations of the cross-plane direction in bulk Bi₂Te₃.

Number of Unit Cells	Length (L_z) (nm)	Number of Atoms
28	≈84	211680
34	≈104	257040
40	≈122	302400
46	≈140	347760

Table S3 System sizes for reverse non-equilibrium molecular dynamics simulations of Te2 twin boundary in Bi₂Te₃.

Number of Unit Cells	Length (L_z) (nm)	Number of Atoms
28	≈84	211680
34	≈104	257040
40	≈122	302400
46	≈140	347760
52	≈159	393120
58	≈177	438480
64	≈195	483840
70	≈213	529200
76	≈232	574560

Figure S1 shows the inverse in-plane and cross-plane lattice thermal conductivity (κ_L) values of Bi₂Te₃ at 300 K for different inverse lengths of simulation cells in the direction parallel to the heat flow (L_z) obtained using rNEMD. We extrapolate the in-plane and cross-plane κ_L values at “infinite” length, which correspond to the κ_L values for bulk Bi₂Te₃, using

$$\frac{1}{\kappa_L(L_z)} = \frac{1}{\kappa_L(\infty)} + \frac{A}{L_z}, \quad (1)$$

where $\kappa_L(\infty)$ is the lattice thermal conductivity for the infinite system length and A is a constant.¹ The extrapolated values and their error bars are given in Tables 2 and 3 in the paper. They were calculated by fitting Eq. (1) for different cell sizes L_z in each of the 5 independent rNEMD runs using a linear least squares fit, and finding the average value and the standard error for the 5 values of $\kappa_L(\infty)$ obtained from those fits. The resulting fit is also shown in Figure S1.

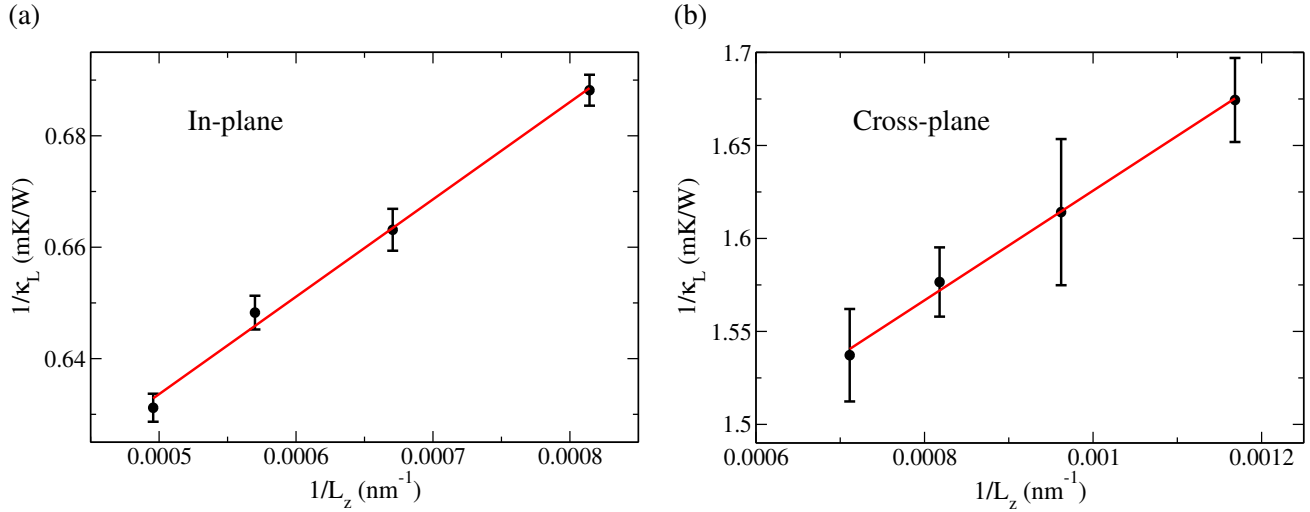


Figure S1 Lattice thermal conductivity (κ_L) of Bi_2Te_3 at 300 K calculated using reverse non-equilibrium molecular dynamics as a function of the simulation cell size in the direction parallel to the heat flow (L_z) for (a) in-plane and (b) cross-plane directions. The error bars shown here represent the standard deviation of the calculated $1/\kappa_L$ values. The linear fits of $1/\kappa_L$ versus $1/L_z$ are also shown in red.

However, Ref. [2] argued that the bulk lattice thermal conductivity should be extrapolated using a different scaling law

$$\kappa_L(L_z) = \kappa_L(\infty) - \frac{A}{L_z}, \quad (2)$$

which has been used to obtain $\kappa_L(\infty)$ from lattice dynamics simulations.^{2,3} Figure S2 shows the in-plane and cross-plane lattice thermal conductivity (κ_L) values of Bi_2Te_3 at 300 K for different inverse lengths of simulation cells in the direction parallel to the heat flow (L_z), as well as the fit to Eq. (2) obtained in the same manner as the fit to Eq. (1). The values of $\kappa_L(\infty)$ for both types of fits are given in Table S4.

The coefficient of determination R^2 of both types of fits is above 0.99, so both Eqs. (1) and (2) fit our calculated lattice thermal conductivity results very well. However, it is physically more appropriate to use Eq. (2) for extrapolation in lattice dynamics calculations, as was done in Refs. [2,3], where no physical boundaries are present in the simulation cells and the size scaling is due to the cutoff of the contribution of low frequency phonons with long mean free paths. In contrast, in rNEMD simulations, energy is transferred from the hot slab to the cold slab through velocity swapping (see Figure 4 of the paper), where the coldest atom in the hot slab and the hottest atom in the cold slab are exchanged. This energy transfer effectively creates interfaces between the bulk material and the hot/cold slab (i.e. the heat source/sink). Therefore, it is more appropriate to use Eq. (1) in rNEMD simulations, which accounts for the phonon boundary scattering due to the interfaces mentioned above.

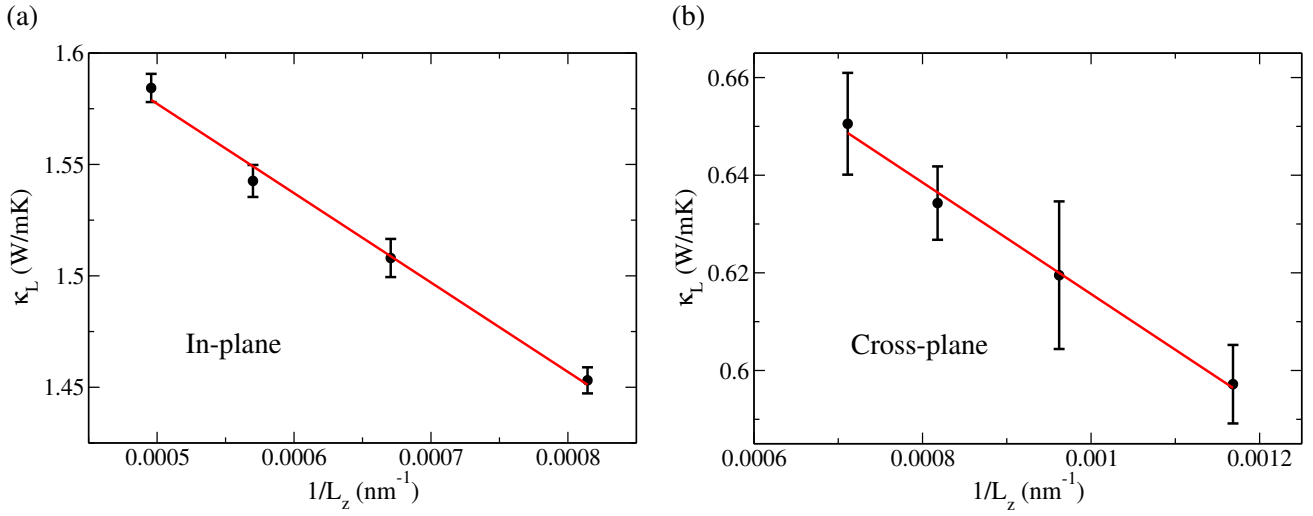


Figure S2 Lattice thermal conductivity (κ_L) of Bi₂Te₃ at 300 K calculated using reverse non-equilibrium molecular dynamics as a function of the simulation cell size in the direction parallel to the heat flow (L_z) for (a) in-plane and (b) cross-plane directions. The error bars shown here represent the standard deviation of the calculated κ_L values. The linear fits of κ_L versus $1/L_z$ are also shown in red.

Table S4: Extrapolated values of lattice thermal conductivity for infinite system sizes, $\kappa_L(\infty)$, using different types of size scaling laws.

	In-plane $\kappa_L(\infty)$ (W/mK)	Cross-plane $\kappa_L(\infty)$ (W/mK)
Fit to Eq. (1)	1.831 ± 0.004	0.751 ± 0.006
Fit to Eq. (2)	1.778 ± 0.002	0.730 ± 0.004

It is important to point out that there are limitations to using Eq. (1) to accurately extrapolate the $\kappa_L(\infty)$ values from NEMD simulations, which are discussed in detail in Ref. [1]. These fits are inaccurate if the size of the system is smaller than the longest significant mean free path.¹ However, in our rNEMD simulations, we are well within the regime where Eq. (2) should give an accurate fit. In first principles simulations of the lattice thermal conductivity of Bi₂Te₃,⁴ it has been shown that the longest significant mean free paths are of the order of 10 nm at 300 K (see Figure 8 of Ref. [4]). Furthermore, the room temperature κ_L values obtained in those calculations are comparable to our rNEMD results.⁴ This implies that the longest significant mean free paths are of the order of 10 nm in our simulations as well. The system lengths used in our rNEMD simulations are of the order of 100 nm (see Tables S1-3). Therefore, our extrapolated rNEMD κ_L values should be fairly accurate.

Figure S3 shows the potential energy per atom for varying cell sizes containing the Bi twin boundary. This plot illustrates that for varying cell sizes a phase transition persists in this system.

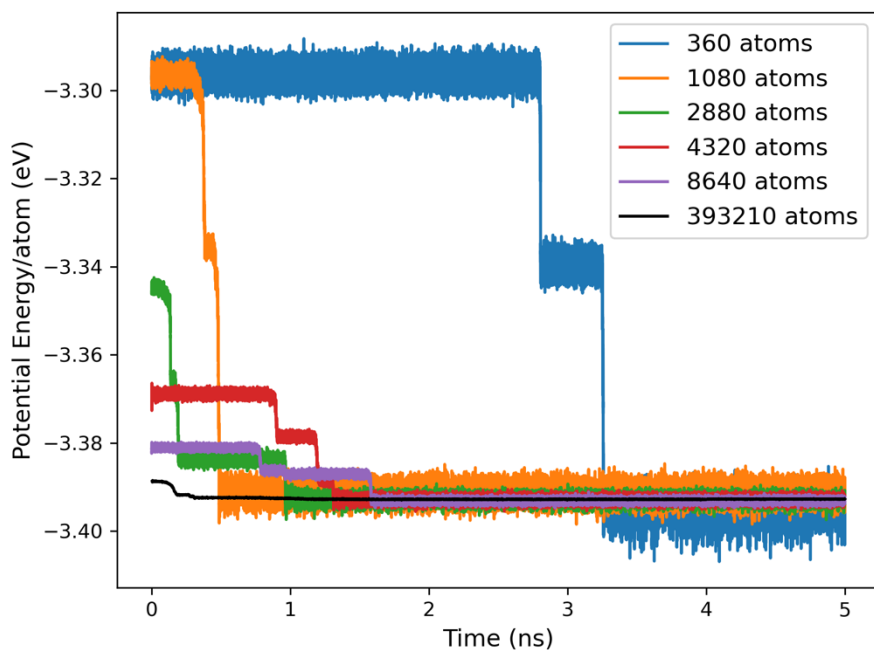


Figure S3 Potential energy per atom at 300 K for varying size supercells containing the Bi twin boundary.

Figure S4 shows the temperature profiles for 5 independent runs of the Te1 twin boundary. Additionally, the average temperature profile (taken over these 5 runs) is shown. Very little deviation is observed across the 5 independent runs.

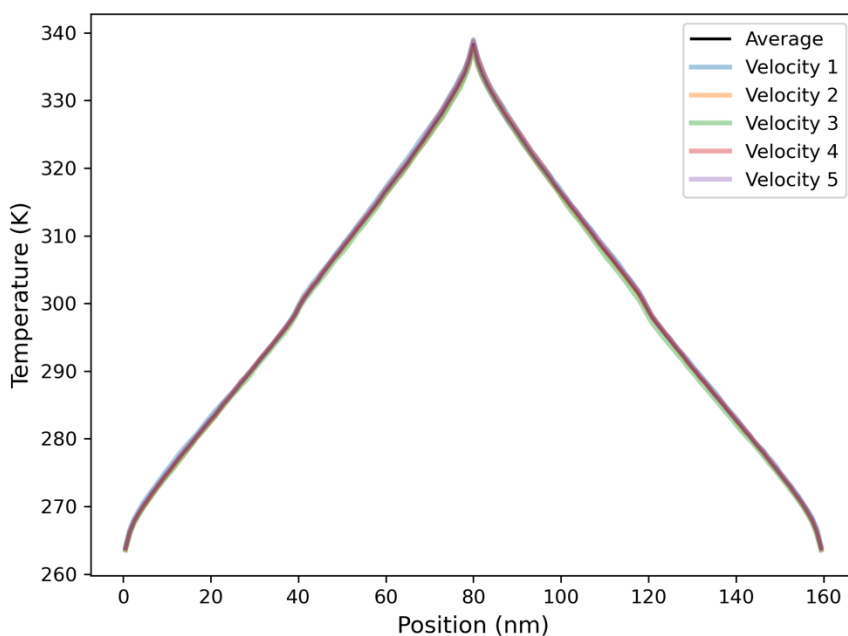


Figure S4 Temperature profiles for the Te1 twin boundary over 5 independent molecular dynamics simulations at 300 K. The system length is $L_z = 159$ nm. The average of the 5 independent runs is also shown.

Figure S5 shows the potential energy per atom of the Bi ‘Structure 1’ and Bi ‘Structure 2’ over 6 ns. From this one can see that Bi ‘Structure 1’ represents a metastable state of Bi ‘Structure

2' which remains stable for long periods. This metastable state remains stable in $\approx 50\%$ of our molecular dynamics simulations. This allows us to calculate thermal boundary resistances for the Bi 'Structure 1' interface as well as the Bi 'Structure 2' interface.

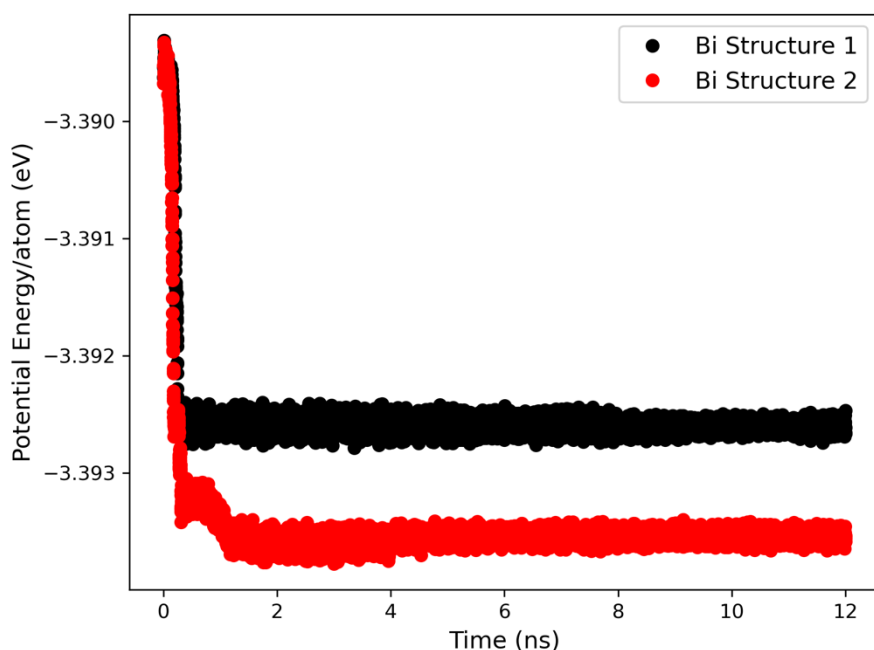


Figure S5 Potential energy per atom at 300 K for Bi twin cells containing 393210 atoms for rNEMD simulations. Bi 'Structure 1' is a metastable state which transforms to Bi 'Structure 2' in $\sim 50\%$ of simulations.

Figure S6 and Table S5 serve to illustrate that in the case of the Bi 'Structure 1' twin boundary we calculate thermal boundary resistance of the system after the phase transition has happened. We plot the temperature profile at 5 ns increments and calculate thermal boundary resistance for those same 5 ns increments to highlight that the thermal boundary resistance is not changing significantly over the course of the run.

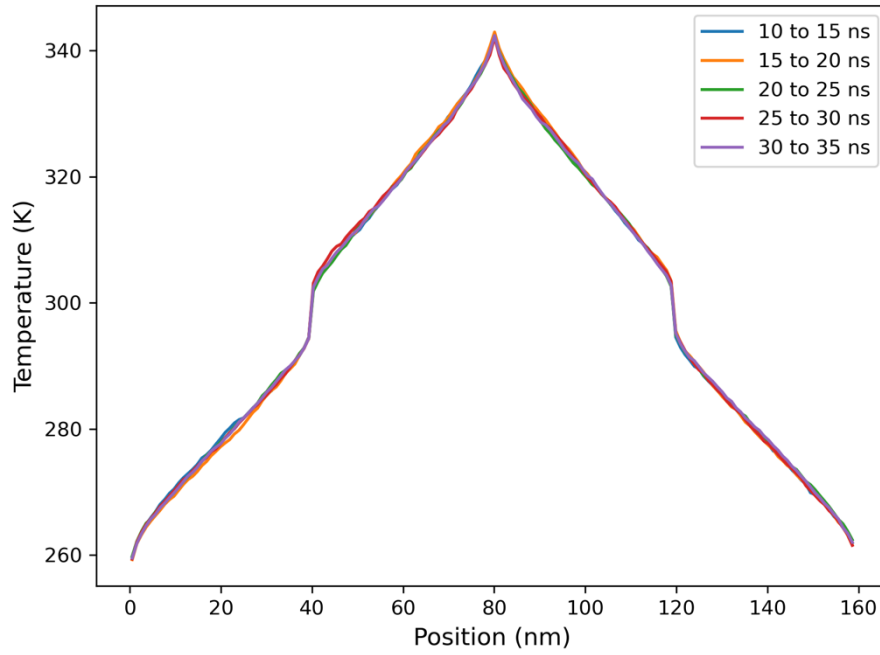


Figure S6 Temperature profile in 5 ns increments for a representative Bi ‘Structure 1’ twin boundary from molecular dynamics simulations at 300 K. The system length is $L_z = 159$ nm.

Table S5 Thermal boundary resistance calculated in 5 ns increments for a structure representative of Bi ‘Structure 1’ whose temperature profiles are shown in Figure S4.

Bi ‘Structure 1’	TBR ($\text{m}^2\text{W/K}$)
10 to 15 ns	1.88E-08
15 to 20 ns	2.00E-08
20 to 25 ns	1.93E-08
25 to 30 ns	2.09E-08
30 to 35 ns	1.89E-08
Average over all segments	1.96E-08

Figure S7 and Table S6 show the same information as Figure S6 and Table S5 but for the Bi ‘Structure 2’ twin boundary.

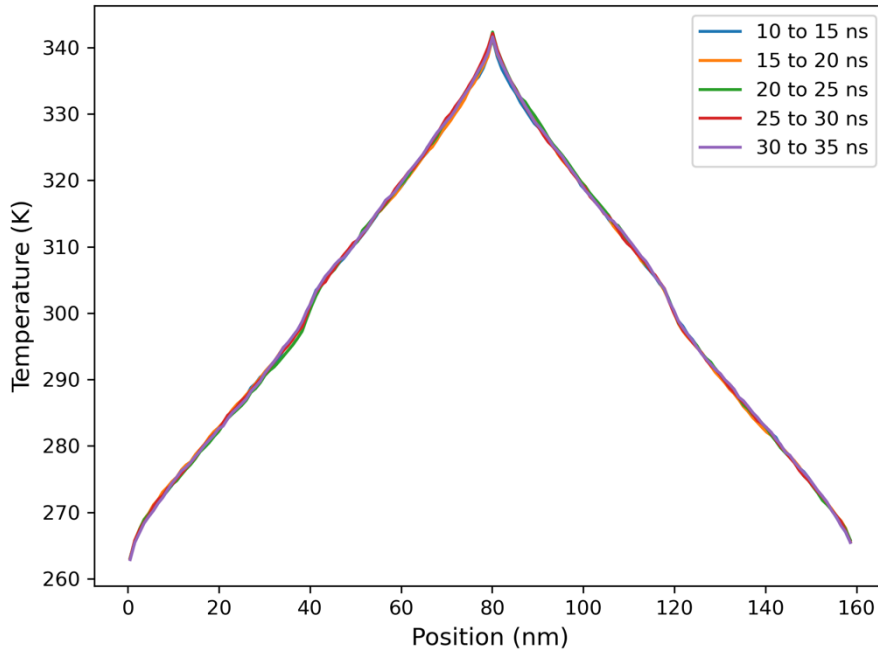


Figure S7 Temperature profile in 5 ns increments for a representative Bi 'Structure 2' twin boundary from molecular dynamics simulations at 300 K. The system length is $L_z = 159$ nm.

Table S6 Thermal boundary resistance calculated in 5 ns increments for a structure representative of Bi 'Structure 2' whose temperature profiles are shown in Figure S5.

Bi 'Structure 2'	Average ($\text{m}^2\text{W/K}$)
10to15	5.30E-09
15to20	5.67E-09
20to25	5.58E-09
25to30	5.07E-09
30to35	5.67E-09
Average over all segments	5.46E-09

Tables S7 and S8 summarise the thermal boundary resistance (TBR) values and temperature discontinuity values (ΔT) for all interfaces investigated in this study.

Table S7 Thermal boundary resistances (TBR) at 300 K for the Te2 and Te1 twin boundaries, and two structures resulting from structural transitions of the Bi twin boundary. Units of $\times 10^{-9} \text{ m}^2\text{K/W}$ apply to the TBR values. All systems have the length of $L_z \approx 159$ nm.

Te2	Te1	Bi 'Structure 1'	Bi 'Structure 2'
4.759 ± 0.083	1.467 ± 0.099	19.470 ± 0.023	5.331 ± 0.031

Table S8 Temperature discontinuity at interface (ΔT) at 300 K for the Te2 and Te1 twin boundaries, and two structures resulting from structural transitions of the Bi twin boundary. Units of K apply to the ΔT values. All systems have the length of $L_z \approx 159$ nm.

Te2	Te1	Bi 'Structure 1'	Bi 'Structure 2'
2.46 ± 0.50 K	0.78 ± 0.06 K	9.78 ± 0.13 K	2.67 ± 0.16 K

Figure S8 shows the values of thermal boundary resistance calculated in this work alongside those calculated by Hsieh and Huang⁵ (using the Huang and Kaviany⁶ interatomic potential).

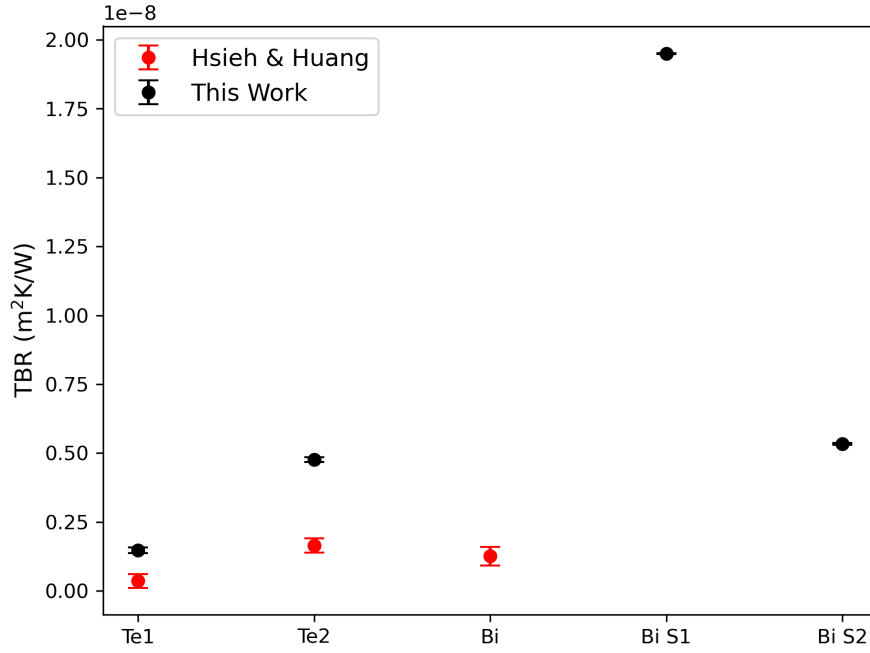


Figure S7 The values of thermal boundary resistance at 300 K obtained in this work are plotted against those obtained by Hsieh and Huang⁵.

Table S9 summarises the effective thermal conductivity of the systems containing twin boundaries (see Figure 9 in the paper and the associated discussion), as well as the percentage reduction of the lattice thermal conductivity when compared to bulk Bi_2Te_3 .

Table S9 Effective lattice thermal conductivity at 300 K of the superlattice-like systems containing twin boundaries (κ_{TB}) with the grain size of $d=79.5$ nm, and the percentage difference of this value compared to the cross-plane lattice thermal conductivity of bulk Bi_2Te_3 (0.751 W/mK).

System	κ_{TB} (W/mK)	Percentage difference to bulk
Te1 TB	0.741 ± 0.002	-1.368
Te2 TB	0.719 ± 0.002	-4.304
Bi 'Structure 1' TB	0.631 ± 0.001	-15.615
Bi 'Structure 2' TB	0.715 ± 0.001	-4.795

References

- [1] D. P. Sellan, E. S. Landry, J. E. Turney, A. J. H. McGaughey, and C. H. Amon, *Physical Review B*, 2010, **81**, 214305.
- [2] K. Esfarjani, G. Chen, and H. T. Stokes, *Physical Review B*, 2011, **84**, 085204.
- [3] D. Aketo, T. Shiga, and J. Shiomi, *Applied Physics Letters*, 2014, **105**, 131901.
- [4] O. Hellman and D. A. Broido, *Physical Review B*, 2014, **90**, 134309.
- [5] I. T. Hsieh and M. J. Huang, *Nanoscale Microscale Thermophysical Engineering*, 2019, 36–47.
- [6] B.-L. Huang and M. Kaviany, *Phys. Rev. B*, 2008, **77**, 125209.